Structure of HfO_2 modified with Y, Gd, and Zr at Ambient Conditions and High Pressures

Brienne Johnson[1], Chris M. Fancher[2+], Dong Hou[1], Jacob L. Jones[1]

[1] Department of Materials Science and Engineering, North Carolina State University, Raleigh, North Carolina, 27695, United States

[2]Neutron Scattering Science Division, Oak Ridge National Laboratory, Oak Ridge, Tennessee, 37830, United States

Abstract: High- resolution and pressure X-ray diffraction measurements were performed to determine the effects of 5% Y-, 3% Gd-, and 50% Zr-substitution on the crystal structure and polymorphism of HfO_2. High resolution experiments at ambient pressure show a mixture of monoclinic and cubic fluorite phases in 5% Y:HfO_2 and 3% Gd:HfO_2, while 50% Zr:HfO_2 formed a monoclinic, single-phase solid solution. Crystallographic refinement using the Rietveld method indicates that Y and Gd substitute for Hf in both the monoclinic and cubic phases. High pressure X-ray diffraction was performed *in situ* up to 31 GPa and shows that the pressure-induced phase transitions were reduced with addition of either Y, Gd, or Zr relative to the transition pressures in the undoped HfO_2. The pressure-induced changes in lattice parameter, relative volume, and spontaneous strain are reported.

Keywords: hafnia, x-ray diffraction, monoclinic, orthorhombic, dopants

Corresponding Author: jacobjones@ncsu.edu

+This manuscript has been authored by UT-Battelle, LLC under Contract No. DE-AC05-00OR22725 with the U.S. Department of Energy. The United States Government retains and the publisher, by accepting the article for publication, acknowledges that the United States Government retains a non-exclusive, paid-up, irrevocable, worldwide license to publish or reproduce the published form of this manuscript, or allow others to do so, for United States Government purposes. The Department of Energy will provide public access to these results of federally sponsored research in accordance with the DOE Public Access Plan (http://energy.gov/downloads/doe-public-access-plan).

Introduction:

The observation of a ferroelectric response in silicon doped HfO_2 (Si:HfO_2) was both surprising and an exciting discovery.[1–5] Unlike perovskite ferroelectric materials, HfO_2 has been demonstrated to maintain ferroelectric properties in <10 nm thick films, and is complementary metal-oxide-semiconductor compatible.[6–8] Since the initial discovery, HfO_2 thin films have been demonstrated to exhibit ferroelectricity when modified with a wide variety of elements, *e.g.,*Si, Al, Zr, Gd, La, Sc, and Y (herein referred to as X:HfO2, where X is the substitutional atom). [2,3,9–15] Ferroelectricity was unexpected in HfO_2 based materials because both the temperature and pressure dependent structures in bulk materials are nonpolar.[16–18] Böscke *et al.* attributed their findings to a stabilization of the polar orthorhombic polymorph ($Pbc2_1$), which has been observed in partially stabilized ZrO_2 at cryogenic temperatures.[1,19,20] Recent scanning transmission electron microscopy work published by Sang *et al.* and Shimizu *et al.* provided direct evidence for the presence of the $Pbc2_1$ phase.[21,22]

In addition to the dopant species, the concentration of each dopant influences the ferroelectric response. For example, the electrical response of Si:HfO_2 and Zr:HfO_2 change from dielectric to ferroelectric and ferroelectric to anti-ferroelectric-like responses with increased Si and Zr concentration, indicating that chemistry is an important factor to promote ferroelectricity.[1,2,23] Simulations have suggested that the polar orthorhombic phase of HfO_2 is close in free energy to the equilibrium phases of HfO_2, indicating that the polar structures may be induced by a distortion of the parent tetragonal phase along its [110] and [100] directions, respectively.[24]

Crystallographic texture, film stresses, and existence of multiple phases hinders the use of classical X-ray diffraction methods for crystallographic structure analysis of HfO_2 films.[25] Bulk materials are advantageous for crystallographic structure analysis as they allow for higher resolution diffraction patterns than thin films. Researchers have investigated the structure of bulk Si:HfO2 using high-resolution and high-pressure diffraction. [26–29] High-resolution x-ray diffraction (HRXRD) was used to determine the effect of Si-substitution and calcination temperature on the crystallographic structures of Si:HfO_2 bulk materials.[26–28] These results demonstrated that, at ambient conditions, Si:HfO_2 is metastable and remains monoclinic with a solubility limit of 9 at.% Si. Si was also found to affect the critical pressure needed to induce the monoclinic to orthorhombic phase transformation.[29]

Prior bulk studies have focused on effects of Si on the ambient and pressure dependent crystallographic structures. More recent literature has identified various other dopants that effectively induce ferroelectricity in HfO_2. In the present work, Y, Gd, and Zr modified HfO_2 bulk materials are investigated to determine how each dopant affects the HfO_2 crystal structure at ambient conditions and at high pressures up to 31 GPa. Gd, Y, and Zr were selected for this investigation due to their relatively high solubility limit (>2 at%) in HfO_2 relative to other dopants such as Si and La. ZrO_2 and HfO_2 form a monoclinic solid solution and has complete solubility. In the compositional regime that optimize ferroelectric responses in films, the bulk phase diagrams of Gd and Y:HfO_2 show a phase mixture of non-polar monoclinic and cubic phases.[12,15] In the present work, we use HRXRD to show that Gd and Y are incorporated into HfO_2, and that as-prepared Y:HfO_2 has a larger cubic volume fraction than Gd:HfO_2 (~15% and ~7% respectively). We will discuss the effect of the secondary phase on the observed pressure induced transitions.

Experimental:

Thin film HfO_2 prepared with 2.3 – 5.2% Y, 2-3% Gd, and 50% Zr are known to show ferroelectric properties with high remanent polarizations (24μC/cm^2, 20μC/cm^2, 16μC/cm^2

respectively).[2,3,9–12,14] Therefore, 5 at% Y-doped HfO_2 (5% Y:HfO_2), 3 at% Gd-doped HfO_2 (3% Gd:HfO_2), and 50 at% Zr-doped HfO_2 (50% Zr:HfO_2) bulk materials were synthesized in powder using conventional solid-state processing, to study these compositions without the complexities of size effects, film strain and interface effects, and using high-resolution diffraction techniques. Commercial powders of HfO_2 (99.95% purity, Alfa Aesar) were reacted using either 2.5 mol% Y_2O_3 (99.95%, Alfa Aesar), 1.5 mol% Gd_2O_3 (99.99%, Alfa Aesar), or 50 mol% ZrO_2 (99.70%, Alfa Aesar). Each powder batch was calcined at 1400°C in air for 4 h. Additional processing details can be found in Ref. [28].

HRXRD patterns were measured at ambient conditions at beamline 11-BM at the Advanced Photon Source (APS), Argonne National Lab using a wavelength of 0.4138950 Å. Discrete detectors are scanned over a 34° 2θ range, with data points collected every 0.001° in 2θ and scan speed of 0.01°/s. High-pressure X-ray diffraction (HPXRD) measurements were conducted at the APS HPCAT beamline 16-BM-B (λ=0.424603 Å). Doped HfO_2 powder samples were hydrostatically pressed using a diamond anvil cell with a Xe gas medium. More information on the high pressure measurements can be found in Ref. [29].

Measured diffraction patterns were analyzed using the Rietveld refinement method in the General Structure Analysis System (GSAS) program with EXPGUI to extract the structural details powder batch.[30,31] Monoclinic (*P*21/*c*), cubic (*Fm*-3*m*) and orthorhombic (*Pbca*) structure models were used as the structure models. The background intensity was modeled using a 10^{th}-order shifted Chebyshev polynomial function. Refined parameters include the zero, profile shape, scale factor, phase fraction, lattice parameters, atomic positions, isotropic displacement parameters, and atomic occupancies. The atomic positions and thermal factors of Hf and each of the substituting dopants were constrained to be equal to each other and. Atomic occupancies were initially set to their ideal value (e.g., 0.5 Zr and 0.5 Hf); however, the total occupancy of each site constrained to equal one in the Rietveld refinement.

Results and Discussion:

Rietveld analysis of HRXRD patterns measured at ambient conditions for Y:HfO_2 and Gd:HfO_2 powders evidences a phase mixture with primary monoclinic and secondary cubic phases. These observations are in agreement with the reported phase diagrams, in which a two-phase region where monoclinic and cubic structures are expected.[32,33] Unlike Gd and Y, Zr has similar physical and chemical properties to those of Hf.[16] These similarities enable full substitution of Zr in HfO_2 results in a single monoclinic phase solid solution.[34] Representative refinement fits of the HRXRD patterns are shown in Fig. 1. The increase in R, which indicates a reduction in goodness of fit, for Gd and Y:HfO_2 is attributed to increased peak asymmetry.

Rietveld refinement results are summarized in Table 1. Both the monoclinic β angle and lattice parameters in both the monoclinic and cubic structures were found to increase in 5% Y:HfO_2 and 3% Gd:HfO_2 with respect to pure HfO_2. This result indicates that the Y and Gd atoms are incorporated into HfO_2. In addition to the incorporation of dopants into the crystal structure, the occupancy results show that the Y and Gd are substituting for Hf in both the cubic and monoclinic structures. Based on the composition of each phase determined from the phase diagrams, at equilibrium, the cubic phase should preferentially incorporate Y and Gd substituents.[32,35] The largest volume increase was found in the 50% Zr:HfO_2: a 0.9% increase in volume.

Undoped HfO_2 has a pressure-induced transformation from monoclinic to orthorhombic, *Pbca*, at ~11GPa.[36,37] Fancher et al. also reported the high-pressure orthorhombic phase of Si:HfO_2 the nonpolar *Pbca*.[29] Thus, in this work, the high-pressure phase is expected as *Pbca*. HPXRD for Y:, Gd:, and Zr:HfO2 evidence that the onset of the orthorhombic transformations shifts to <9

GPa, <7 GPa, and <7 GPa, respectively. The results demonstrate that each dopant changes the critical pressure to induce the transition, which is consistent with previously reported Si-doped HfO_2 results.[29] It should be noted that evidence for the onset of the orthorhombic structure was observed near 7 GPa in Gd:HfO_2; however, the patterns of orthorhombic and cubic are similar which limits the detection of the initial onset. While the orthorhombic phase is first detected near 7 GPa in Gd and Zr:HfO_2, the HPXRD demonstrates that Zr:HfO_2 dominantly orthorhombic while Gd:HfO_2 is a mixture of orthorhombic and monoclinic. The orthorhombic phase does not become dominant in Gd:HfO_2 until ~9 GPa, while Y:HfO_2 requires even higher pressures ~11 GPa. Similar to Zr:HfO_2, Prior work has reported that the orthorhombic phase became the dominant phase at ~7 GPa in Si:HfO_2.[29] These results suggest that the presence of a cubic volume fraction stabilizes the as-processed phases.

HPXRD data were further analyzed to extract information about the lattice parameters for each phase. The lattice parameters of Y, Gd, and Zr: HfO_2 at high pressures for the monoclinic (a_M, b_M, and c_M) and orthorhombic, *Pbca*, (a_O, b_O, and c_O) phases are shown in Fig. 2. Previously reported HPXRD results by Fancher *et al*. on Si-modified HfO_2, indicated that the lattice parameters along the b_M and a_M crystallographic directions appear to continuously transition into the a_O and c_O crystallographic directions, respectively.[29] Similar to the Si:HfO_2 behavior with increased pressure, the crystallographic directions of the lattice parameters in the present work appear continuous along the b_M and a_O directions with each of the dopants, but the a_M direction does not continuously transition into the c_O direction in Y:HfO_2. Instead, the a_M appears to transition into the b_O direction.

Pressure dependent lattice parameters were used to determine the changes in the relative volume and spontaneous strain with applied pressure. Details for the calculation of spontaneous strain in the monoclinic and orthorhombic structures can be found in Ref. [38]. A constant change in relative volume with increasing pressure is found for both the orthorhombic and monoclinic structures for all powders, shown in Fig. 3a. These results evidence that the monoclinic relative volume decreases more strongly with pressure than the orthorhombic, indicating that the monoclinic phase is more compressible than the orthorhombic phase. The slope of the change in volume is independent of dopant species suggesting that the dopants do not significantly affect the elastic properties of the different phases. Similar to the pressure dependent relative volume, the spontaneous strain for both the monoclinic and orthorhombic phases (Fig. 3b) are independent of dopant species. Increasing the pressure results in dissimilar responses in the monoclinic and orthorhombic structures: with increased pressure, a reduction in the spontaneous strain of the monoclinic structure is observed, while an increase in the spontaneous strain of the orthorhombic structure is observed. This phenomenon is explained by Fancher *et al*., who stated that a decrease in spontaneous strain in the monoclinic structure indicates that the monoclinic structure is becoming less distorted at higher pressures, while the increasing spontaneous strain of the orthorhombic structure with increasing pressure is due to the anisotropic compressibility of the principle axes of the orthorhombic structure.[29]

The present results of the high-resolution data of Y-, Gd, and Zr-modified HfO_2 powders show that Y and Gd substitution stabilize a coexistence of the cubic and monoclinic fluorite phases, while Zr substitution results in a monoclinic phase solid solution. Each substituent changed the pressure-induced phase transitions. Both Y and Gd have an ionic radius that is ~16% larger than that of Hf and are trivalent cations (+3 state). The substitution of trivalent Y and Gd cations into HfO_2 results in the formation of oxygen vacancies to maintain charge neutrality, which are randomly distributed throughout the crystal structure.[39] Although Y and Gd substitution stabilizes the formation of the cubic fluorite phase, once the pressure induced orthorhombic phase forms, it is difficult to determine if the cubic phase remains due to their similarities in crystal structure. It is believed that, above 10 GPa, the only phase present is the orthorhombic phase. For the case of substitution with Zr, a monoclinic solid solution is formed at ambient conditions. The retention of the monoclinic phase in the solid solution is due to the similarities in valency, ionic radii, electronegativity, and crystal structure of HfO_2 and ZrO_2. Although HfO_2 and ZrO_2 have similar crystal structures, the volume of the monoclinic HfO_2 crystal structure is slightly smaller than ZrO_2 because the Hf^{4+} ion is smaller than the Zr^{4+}ion. The ionic size difference is due to the lanthanide contraction, which occurs because there are no outer electrons added to compensate for the increased nuclear charge.

While the specific mechanism, or mechanisms, to induce the polar structure are not well understood, computational work has informed the pathways to induce the polar phase. Materlik *et al.* suggest that surface energy is a dominant factor that controls crystallographic structure.[40] Reyes-Lilo *et al.* suggested that tetragonal ZrO_2 can undergo a first order electric field induced phase transition to polar orthorhombic (field on).[41] When interpreting diffraction patterns in these systems, it should be noted that the diffraction patterns of the cubic and tetragonal phases of HfO_2 and ZrO_2 are similar. The limited resolution of the high-pressure experiment (shown in Fig S1.) prohibited determining if hydrostatic pressure induced a cubic to tetragonal transition in Y: and Gd:HfO_2. Thus far, only anisotropic stresses (electric field and deviatoric stress) that have been predicted to induce a ferroelectric phase from the non-polar tetragonal.[24,41] The isotropic nature of hydrostatic pressure might be inadequate to induce the polar phase. A reduction in the critical pressure to induce the nonpolar phase suggests that modifying the chemistry of HfO_2 (elemental substitution and defects) lowers the energy barriers to induce structural transitions. The correlation between onset pressure to induce the non-polar orthorhombic phase and cubic phase fraction might indicate that the presence of a secondary phase helps to stabilize as-processed structures in films. In films, however, surface energy will likely be a strong determining factor on the development of phases.

Generally, it can be concluded, based on previously reported Si:HfO_2[29] results and the Y-, Gd-, and Zr:HfO_2 results reported here, that substitution in HfO_2 can change the monoclinic to orthorhombic pressure induced phase transition from ~11 GPa to between 5-9 GPa. While all chemistries lowered the critical pressure to induce the non-polar orthorhombic phase, HPXRD data indicate that the onset pressure increases in samples with higher cubic volume fraction. This result indicates that presence of a secondary phase might stabilize as-processed phase mixtures. The presence of a cubic volume fraction does not impact the pressure dependent lattice contraction, indicateing that neither chemical modification or phase present affects the mechanical properties of the monoclinic or orthorhombic phases.

The authors gratefully acknowledge funding from the Army Research Office through contract number W911NF-15-1-0593. HPCAT operations at sector 16 of the APS are supported by DOE-NNSA under Award No. DE-NA0001974 and DOE-BES under Award No. DE-FGo2-99ER45775, with partial instrumentation funding by NSF. The high-resolution diffraction measurements conducted at beamlines 11-BM-B was supported by the U.S. Department of Energy, Office of Science, Office of Basic Energy Sciences, under contract No. DE-AC02-06CH11357. The authors acknowledge Guoyin Shen and Lingang Bai for the diamond anvil cell expertise. D.H. thanks financial support of China Scholarship Council. C.M.F acknowledges support at the Oak Ridge National Laboratory by the DOE Office of Science User Facilities (DOE DE-AC05-00OR22725).

References

[1] T.S. Böscke, J. Müller, D. Bräuhaus, U. Schröder, and U. Böttger, Appl. Phys. Lett. **99**, 102903 (2011).

[2] M.H. Park, Y.H. Lee, H.J. Kim, Y.J. Kim, T. Moon, K. Do Kim, J. Müller, A. Kersch, U. Schroeder, T. Mikolajick, and C.S. Hwang, Adv. Mater. n/a (2015).

[3] D. Martin, J. Müller, T. Schenk, T.M. Arruda, A. Kumar, E. Strelcov, E. Yurchuk, S. Müller, D. Pohl, U. Schröder, S. V. Kalinin, and T. Mikolajick, Adv. Mater. **26**, 8198 (2014).

[4] H. Yu, C.-C. Chung, N. Shewmon, S. Ho, J.H. Carpenter, R. Larrabee, T. Sun, J.L. Jones, H. Ade, B.T. O'Connor, and F. So, Adv. Funct. Mater. **27**, 1700461 (2017).

[5] D. Martin, E. Yurchuk, S. Müller, J. Müller, J. Paul, J. Sundquist, S. Slesazeck, T. Schlösser, R. van Bentum, M. Trentzsch, U. Schröder, and T. Mikolajick, Solid. State. Electron. **88**, 65 (2013).

[6] Z. Fan, J. Chen, and J. Wang, J. Adv. Dielectr. **06**, 1630003 (2016).

[7] T.S. Böescke, J. Müller, D. Bräuhaus, U. Schröder, and U. Böttger, in *Tech. Dig. - Int. Electron Devices Meet. IEDM* (2011), pp. 547–550.

[8] U. Schroeder, S. Mueller, J. Mueller, E. Yurchuk, D. Martin, C. Adelmann, T. Schloesser, R. van Bentum, and T. Mikolajick, ECS J. Solid State Sci. Technol. **2**, N69 (2013).

[9] J. Müller, U. Schröder, T.S. Böscke, I. Müller, U. Böttger, L. Wilde, J. Sundqvist, M. Lemberger, P. Kücher, T. Mikolajick, and L. Frey, J. Appl. Phys. **110**, 114113 (2011).

[10] J. Müller, T.S. Böscke, D. Bräuhaus, U. Schröder, U. Böttger, J. Sundqvist, P. Kücher, T. Mikolajick, and L. Frey, Appl. Phys. Lett. **99**, 112901 (2011).

[11] S. Müller, J. Müller, A. Singh, S. Riedel, J. Sundqvist, U. Schröder, and T. Mikolajick, Adv. Funct. Mater. **22**, 2412 (2012).

[12] S. Müller, C. Adelmann, A. Singh, S. Van Elshocht, U. Schröder, and T. Mikolajick, ECS J.

Solid State Sci. Technol. **1**, N123 (2012).

[13] L. Xu, S. Shibayama, K. Izukashi, T. Nishimura, T. Yajima, S. Migita, and A. Toriumi, Tech. Dig. - Int. Electron Devices Meet. IEDM 25.2.1 (2017).

[14] U. Schroeder, E. Yurchuk, J. Müller, D. Martin, T. Schenk, P. Polakowski, C. Adelmann, M.I. Popovici, S. V. Kalinin, and T. Mikolajick, Jpn. J. Appl. Phys. **53**, 08LE02 (2014).

[15] T. Olsen, U. Schröder, S. Müller, A. Krause, D. Martin, A. Singh, J. Müller, M. Geidel, and T. Mikolajick, Appl. Phys. Lett. **101**, 082905 (2012).

[16] J. Wang, H.P. Li, and R. Stevens, J. Mater. Sci. **27**, 5397 (1992).

[17] J.E. Lowther, J.K. Dewhurst, J.M. Leger, and J. Haines, Phys. Rev. B **60**, 14485 (1999).

[18] J. Kang, E.-C. Lee, and K. Chang, Phys. Rev. B **68**, 054106 (2003).

[19] E.H. Kisi, C.J. Howard, and R.J. Hill, J. Am. Ceram. Soc. **72**, 1757 (1989).

[20] C.J. Howard, E.H. Kisi, R.B. Roberts, and R.J. Hill, J. Am. Ceram. Soc. **73**, 2828 (1990).

[21] X. Sang, E.D. Grimley, T. Schenk, U. Schroeder, and J.M. LeBeau, Appl. Phys. Lett. **106**, 162905 (2015).

[22] T. Shimizu, K. Katayama, T. Kiguchi, A. Akama, T.J. Konno, and H. Funakubo, Appl. Phys. Lett. **107**, 032910 (2015).

[23] J. Müller, T.S. Böscke, U. Schröder, S. Mueller, D. Bräuhaus, U. Böttger, L. Frey, and T. Mikolajick, Nano Lett. **12**, 4318 (2012).

[24] T.D. Huan, V. Sharma, G.A. Rossetti, R. Ramprasad, T. Doan Huan, V. Sharma, G.A. Rossetti, and R. Ramprasad, Phys. Rev. B **90**, 064111 (2014).

[25] M.H. Park, T. Schenk, C.M. Fancher, E.D. Grimley, C. Zhou, C. Richter, J.M. Lebeau, J.L. Jones, T. Mikolajick, and U. Schroeder, J. Mater. Chem. C **5**, (2017).

[26] L. Zhao, D. Hou, T.-M. Usher, T. Iamsasri, C.M. Fancher, J.S. Forrester, T. Nishida, S.

Moghaddam, and J.L. Jones, J. Alloys Compd. **646**, 655 (2015).

[27] D. Hou, C.M. Fancher, L. Zhao, G. Esteves, and J.L. Jones, J. Appl. Phys. **117**, 244103 (2015).

[28] L. Zhao, M. Nelson, H. Aldridge, T. Iamsasri, C.M. Fancher, J.S. Forrester, T. Nishida, S. Moghaddam, and J.L. Jones, J. Appl. Phys. **115**, 034104 (2014).

[29] C.M. Fancher, L. Zhao, M. Nelson, L. Bai, G. Shen, and J.L. Jones, J. Appl. Phys. **117**, 234102 (2015).

[30] R.B. Larson, A.C.; Von Dreele, *Los Alamos National Laboratory Report No. LAUR* (2004).

[31] B.H. Toby and IUCr, J. Appl. Crystallogr. **34**, 210 (2001).

[32] F. Spiridonov, L. Komissarova, A. Kocharov, and V. Spitsyn, Russ. J. Inorg. Chem. **14**, 1332 (1969).

[33] R.L. Magunov, G.L. Shklyar, and V.F. Katridi, Inorg. Mater. **25**, 1035 (1989).

[34] T. Yamada, M. Mizuno, T. Ishizuka, and T. Noguchi, Adv. Ceram. Mater. **24B**, 959 (1988).

[35] P. Duran, Ceramurg. Int. **3**, 137 (1977).

[36] J.M. Leger, A. Atouf, P.E. Tomaszewski, and A.S. Pereira, Phys. Rev. B **48**, 93 (1993).

[37] C.M. Fancher, L. Zhao, M. Nelson, L. Bai, G. Shen, and J.L. Jones, J. Appl. Phys. **117**, 234102 (2015).

[38] S.A.T. Redfern and E. Salje, J. Phys. C Solid State Phys. **21**, 277 (1988).

[39] M.S. Khan, M.S. Islam, and D.R. Bates, J. Mater. Chem. **8**, 2299 (1998).

[40] R. Materlik, C. Künneth, and a. Kersch, J. Appl. Phys. **117**, 134109 (2015).

[41] S. Reyes-Lillo, K. Garrity, and K. Rabe, Phys. Rev. B **90**, 1 (2014).

[42] R.W.G. Wyckoff, Second Ed. Intersci. Publ. New York, New York Cryst. Struct. **1**, 239 (1963).

[43] P.W.R. Ruh, R.; Corfield, J. Am. Ceram. Soc. **53**, 126 (1970).

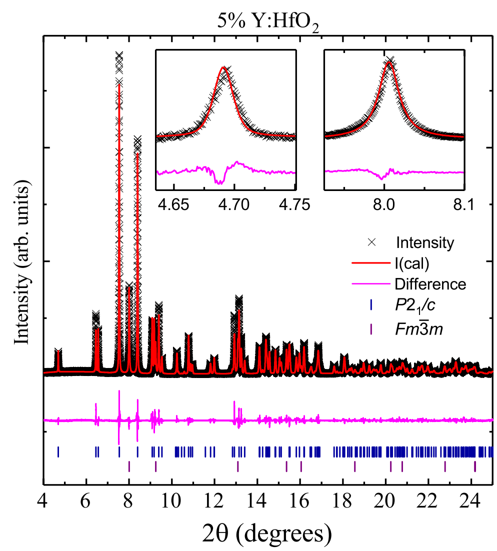
5% Y:HfO$_2$
Intensity (arb. units)
2θ (degrees)
Intensity
I(cal)
Difference
$P2_1/c$
$Fm\bar{3}m$
4.65
4.70
4.75
8.0
8.1
4
6
8
10
12
14
16
18
20
22
24

(a)

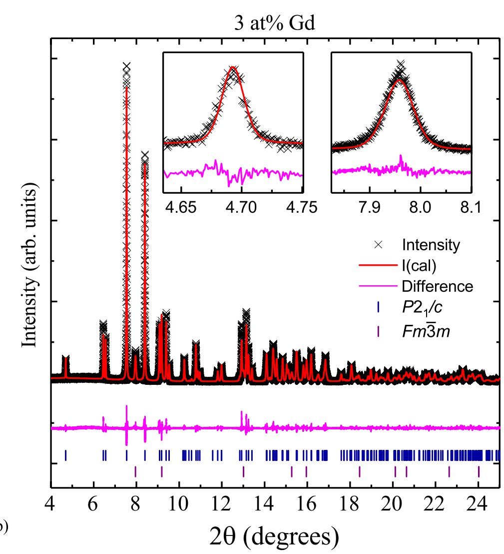
3 at% Gd
Intensity (arb. units)
2θ (degrees)
Intensity
I(cal)
Difference
$P2_1/c$
$Fm\bar{3}m$
4.65
4.70
4.75
7.9
8.0
8.1
4
6
8
10
12
14
16
18
20
22
24

(b)

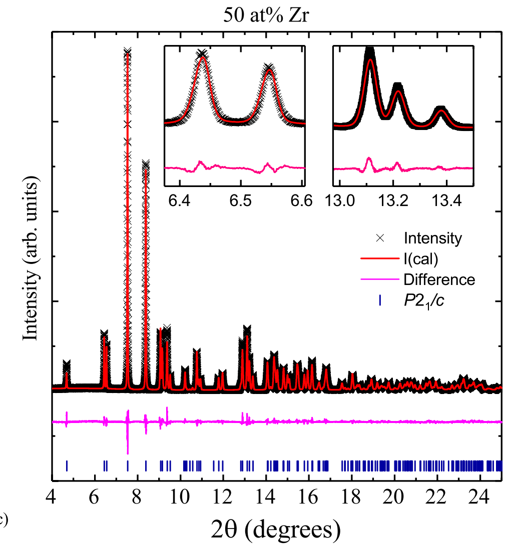

(c)

Fig. 1. HRXRD patterns and the best-fit modeled pattern from the Rietveld method of (a) 5%Y:HfO2, (b) 3%Gd:HfO2, and (c) 50%Zr:HfO2 with identified phases and refinement results. Insets show zoomed regions for representative reflections to highlight the Rietveld analysis.

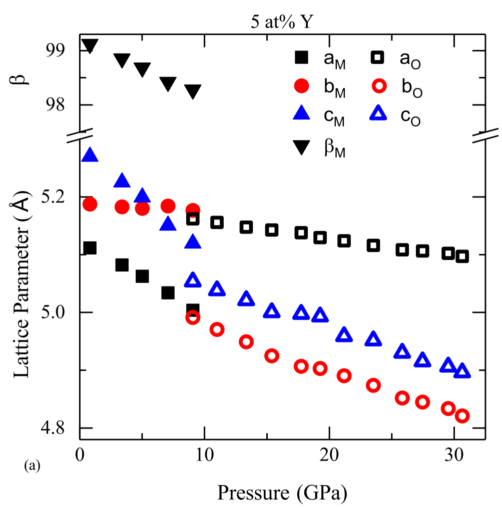

(a)

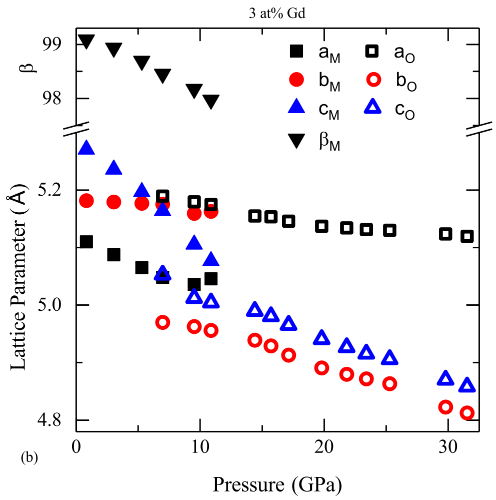

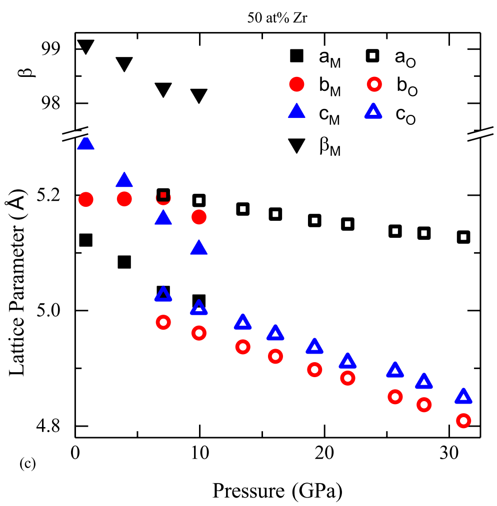

Fig.2. Pressure induced changes in the lattice parameters (Å) and β angle (°) of monoclinic (solid) and orthorhombic (open) crystal structures of (a) 5%Y:HfO2 (b) 3%Gd:HfO2 (c) 50%Zr:HfO2.

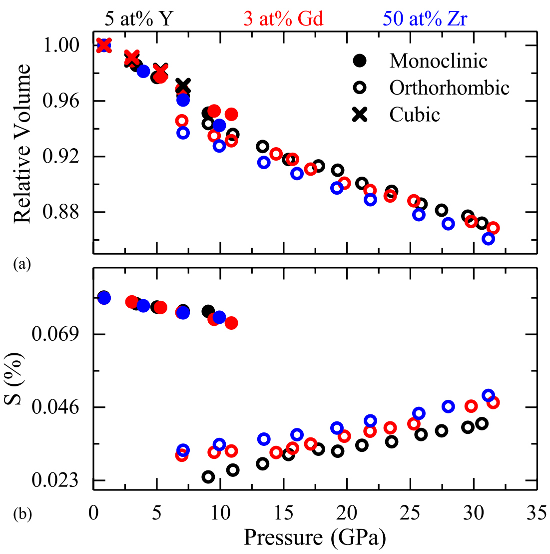

Fig. 3. Pressure induced changes in the (a) relative volume and (b) spontaneous strain (S) of monoclinic (solid) and orthorhombic (open) structures up to 31GPa.

Table 1: Summary of refined lattice parameters, occupancies, fractional coordinates, phase fractions, and goodness of fit at ambient pressure

	Undoped HfO_2 [42,43]	5%Y:HfO_2	3%Gd:HfO_2	50%Zr:HfO_2
Lattice Parameters (*P2₁/c*) (Å)				
a	5.1156	5.12070(3)	5.121796(32)	5.13300(9)
b	5.1722	5.17387(6)	5.174242(34)	5.18999(2)
c	5.2948	5.29424(1)	5.297197(41)	5.30722(7)
β	99.18	99.22(1)	99.21(2)	99.18(1)
Cell Volume (*P2₁/c*) (Å³)	138.30	138.46	138.54	139.55
Lattice Parameters (*Fm-3m*) (Å)				
a	5.115	5.13389(4)	5.166214(5)	
b	5.115	5.13389(4)	5.166214(5)	
c	5.115	5.13389(4)	5.166214(5)	
Cell Volume (*Fm-3m*) (Å³)	133.82	135.56	137.87	
Hf (Y, Gd, Zr) site (*P2₁/c*)				
x	0.2755	0.27565(5)	0.27562(4)	0.27619(1)
y	0.0397	0.03978(2)	-0.46029(4)	0.04067(3)
z	0.208	0.20731(8)	0.20776(3)	0.20406(1)
O₁ site (*P2₁/c*)				
x	0.0742	0.06733(6)	0.047773(7)	0.07408(6)
y	0.3316	0.32627(9)	0.25671(3)	0.33318(4)
z	0.3467	0.34327(4)	0.48326(3)	0.34667(8)
O₂ site (*P2₁/c*)				
x	0.4487	0.44636(2)	-0.06900(9)	0.45072(3)
y	0.7581	0.75499(2)	0.17355(3)	0.75624(4)
z	0.4801	0.48087(1)	0.65422(5)	0.48202(8)
Hf (Y, Gd, Zr) site (*Fm-3m*)				
x	0	0	0	
y	0	0	0	
z	0	0	0	
O₁ site (*Fm-3m*)				
x	0.25	0.25	0.25	
y	0.25	0.25	0.25	
z	0.25	0.25	0.25	
Hf Occupancy (*P2₁/c*)	1	0.981(1)	0.952(4)	0.567(7)

Dopant Occupancy (*P2₁/c*)		0.019(4)	0.047(4)	0.432(3)
Hf Occupancy (*Fm-3m*)	1	0.977(27)	0.948(4)	
Dopant Occupancy (*Fm-3m*)		0.022(27)	0.051(6)	
Phase Fractions (%)				
$P2_1/c$		84.8258(7)	92.9156(2)	
Fm-3m		15.1746(4)	7.0849(4)	
Profile Fit				
R_{wp}		12.96%	12.84%	10.35%
R_p		10.15%	10.15%	7.97%
χ^2		3.748	1.485	2.34